Intermediate scale band gap fluctuations in ultrathin $CuInGaSe_2$ absorber layers

J. de Wild [1,2,3], D.G. Buldu [1,2,3], T. Kohl[1,2,3], G. Birant [1,2,3], G. Brammertz [1,2,3], M. Meuris[1,2,3], J. Poortmans[1,3,4,5], B. Vermang[1,2,3]

[1] Institute for Material Research (IMO), Hasselt University (partner in Solliance), Wetenschapspark 1, 3590 Diepenbeek, Belgium
[2] IMOMEC, imec (partner in Solliance), Wetenschapspark 1, 3590 Diepenbeek, Belgium.
[3] EnergyVille 2, Thor Park 8320, 3600 Genk, Belgium
[4] imec (partner in Solliance), Kapeldreef 75, 3001 Leuven, Belgium
[5] Department of Electrical Engineering, KU Leuven, Kasteelpark Arenberg 10, 3001 Heverlee, Belgium

Abstract
Ultrathin single and 3-stage $Cu(In,Ga)Se_2$ absorber layers were analyzed with room temperature photoluminescence (PL) spectra. An anomalous blueshift was observed upon increasing carrier injection for both samples. This blueshift was attributed to the presence of band gap fluctuations that are of the same order as the minority carrier diffusion length. From time resolved measurements a diffusion length of a few 100 nm's was deduced. The single stage spectrum consists of 2 peaks and the sample was therefore also analyzed by hyperspectral imaging, providing lateral PL and reflectance data with 1 µm resolution. Marginal variations were observed in the PL yield and spectra. This homogeneity could again be attributed to intermediate scale of the band gap fluctuation with an upper limit of 1 µm for the scale of the lateral band gap fluctuations. The 2 peaks in the PL spectra of the single stage sample could be attributed to interference and correction methods were applied. The band gap fluctuations were extracted for the 3-stage and single stage sample and were 45 meV and 72 ± 3 meV, respectively. It is suggested that this difference is attributed to the smaller grains and larger amount of grain boundaries in the single stage sample.

I. INTRODUCTION

Photoluminescence (PL) is a powerful tool to analyze semiconductor materials on their opto-electrical properties. Information about defects in the band gap, quasi fermi level splitting, potential fluctuations can be deduced from photoluminescence spectra[1,2]. Often, intensity and temperature dependent measurements are done to gain information about the origin of the non-idealities in the material. At room temperature (RT) specifically, additional parameters as optical diode factor, sub band gap absorptivity and band gap fluctuations can be deduced[3–5]. At RT the luminescence should come from the conduction to valence band transition only and has its peak maximum at $1/2k_BT$ above the band gap[1]. However, for poly-crystalline thin films like $CuInGaSe_2$ the interpretation may become increasingly more difficult due to charged defects, band gap fluctuations, extended tail states, etc. causing a shift and/or broadening of the PL peak at room temperature.
When the band gap is not constant, for instance in CIGS due to the presence of a Ga gradient, the peak will be broadened and may even emit below the band gap[6]. In kesterite, the emission is below the calculated band gap, most likely due to a significant amount of tail states[7]. Sometimes several peaks are measured at RT. This can be because of secondary phases i.e. In/Ga segregation in CIGS or ZnSe in kesterite[8,9], but also due to deep defects as is the case in copper rich CI(G)S(e)[10]. Another reason for the appearance of multiple peaks in room temperature PL spectra is the presence of interference fringes[11].

In this contribution we will explain 2 anomalies observed in our PL spectra of ultrathin co-evaporated absorber layers. 1) blue shift upon increasing carrier injection at RT and 2) the appearance of two clearly distinguishable peaks in the PL spectra of copper poor grown absorber layers[12,13]. We will show that the blue shift can be explained by intermediate scale band gap fluctuations generally and the 2 peaks in single stage grown co-evaporated CIGS layers by interference fringes specifically.

II. ROOM TEMPERATURE PHOTOLUMESCENCE

A. Band gap fluctuations

At room temperature the PL emission comes from the conduction to the valence band transition and is described by Planck's law in non-equilibrium. The derivation is developed by Lasher-Stern-Würfel and will be referred to as the LSW equation[14,15]. The PL emission can be described by an absorptivity term and an adapted Boltzmann term:

$$I_{PL}(E) = \frac{2\pi}{h^3c^2}\frac{E^2 a(E)}{\exp\left(\frac{E-\Delta\mu}{k_B T}\right)-1} \quad (1)$$

In here $\Delta\mu$ is the quasi fermi level splitting (qfls), k_B the Boltzmann constant and T the temperature in Kelvin. $a(E)$ is the absorptivity, which is 0 below the band gap and 1 above the band gap for an ideal semiconductor. In real semiconductors, the band edge is not a step function and the absorption below the band gap has a certain distribution depending on the origin of the states near the band edge[16]. For the derivation of the LSW equation, the absorption profile near the band edge is assumed to not affect the qfls, i.e. the qfls is constant. It is possible though that when the band gap varies spatially in the semiconductor it also affects the qfls. This is graphically predicted in figure 1. The emission can then be described by a band gap fluctuations model. Whether the qfls is constant or varies, depends on the scale of the fluctuations in relation to the diffusion length. In here we shortly summarize what this means for the PL spectra. For the derivation we refer to the paper by Rau et. al.[5]

The relationship between the scale of the fluctuation L_g and the diffusion length L_μ is given by a parameter β:

$$\beta = \frac{1}{\left((L_\mu/L_g)^2+1\right)^{dim/4}} \quad (2)$$

in which *dim* is the spatial dimension the fluctuations are expected which is 1, 2 or 3. The two extremes, i.e. $\beta = 1$ and $\beta = 0$, belong to the large ($L_g \gg L_\mu$) and small ($L_g \ll L_\mu$) scale fluctuations respectively. When L_μ is of the same order as L_g the parameter β is between 1 and 0, the intermediate scenario. The generalized emission profile for all length scales is then given by:

$$I_{PL}(E) = erfc\left(\frac{\bar{E}_g - E + \beta\sigma_g^2/k_B T}{\sqrt{2}\sigma_g}\right) E^2 exp\left(-\frac{E-\mu_0-\beta\bar{E}_g}{k_B T} + \frac{(\beta\sigma_g)^2}{2(k_B T)^2}\right) \quad (3)$$

In here σ_g is the amount of band gap fluctuations and $\bar{E}_g$ the mean band gap. The absorptivity $a(E)$ is presented as an error function. For $\beta = 0$, the LSW equation returns with $a(E) = erfc((\bar{E}_g - E)/\sqrt{2}\sigma_g)$. This is the case were the spatial band gap fluctuations are small compared to the diffusion length and therefore the qfls is constant (figure 1, μ_s).

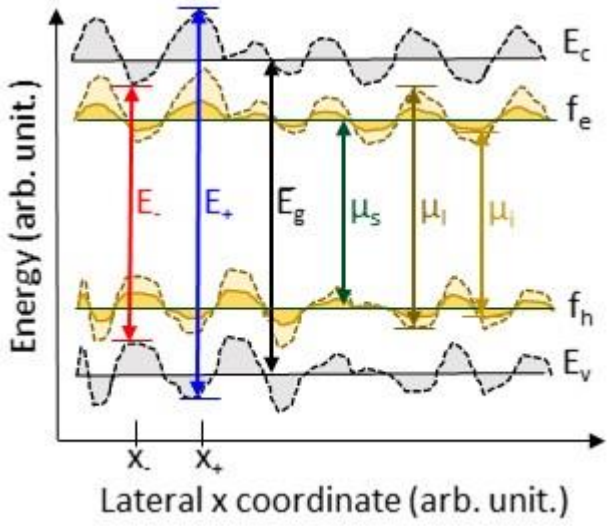

FIG. 1. Graphical representation of the lateral band gap fluctuations. E_- is a low band gap at position x_- and E_+ a higher band gap at position x_+. $\overline{E}_g$ is the mean band gap. Depending on the length scale of the fluctuations (described in the text), the quasi fermi levels follow the local band gaps (dashed line), the average band gap only (solid dark green line) or is somewhere between the 2 extremes (yellow line). f_e is the electron fermi level, f_h the hole fermi level, E_v the valence band and E_c conduction band energy heights.

We calculated some PL spectra to see how the PL yield changes upon these small variations in the band gap using the LSW equation. For this we assumed that the band edge at a local position x_{loc} with E_{loc} is described by a step function for the absorptivity. The band gap was varied from 1.1 to 1.2 eV in steps of 10 meV. We simulated the two extremes: qfls is constant and has a value of 0.7 eV (small scale fluctuations) and the qfls varies with the band gap according to $E_{g,loc} - \mu_l = 0.4\ eV$ (large scale fluctuations). The results are shown in figure 2. For small scale fluctuations the PL intensity decreases exponentially when the band gap increases. This makes sense, as the exponential part in the LSW equation does not change, while the absorptivity term shifts the PL peak to higher energy. Hence, a higher band gap with same qfls, results in decreased PL yield. For the large scale fluctuations, the PL peak simply shifts over the energy range to higher energy, but hardly changes yield. The small increase is merely due to the E^2 factor in the equation. Thus, from this straighforward modelling we can expect large variations in spatial PL yield if the band gap fluctuations are small scale, and marginal variations in the spatial PL yield if the band gap fluctuations are large scale. Of course this also depends on the spot size as the spot size determines the lateral resolution the band gap fluctuations can be measured. Few studies have shown PL spectra on a microscopic scale. In these studies the changes in intensity varied about a factor 4 for CIGSe to 10 for CIS. This could imply small scale band gap fluctuations with constant qfls or changes in qfls with a constant band gap [17,18]. To be able to differentiate between the two options it is crucial to know the exact band gap at the position the PL is emitted.

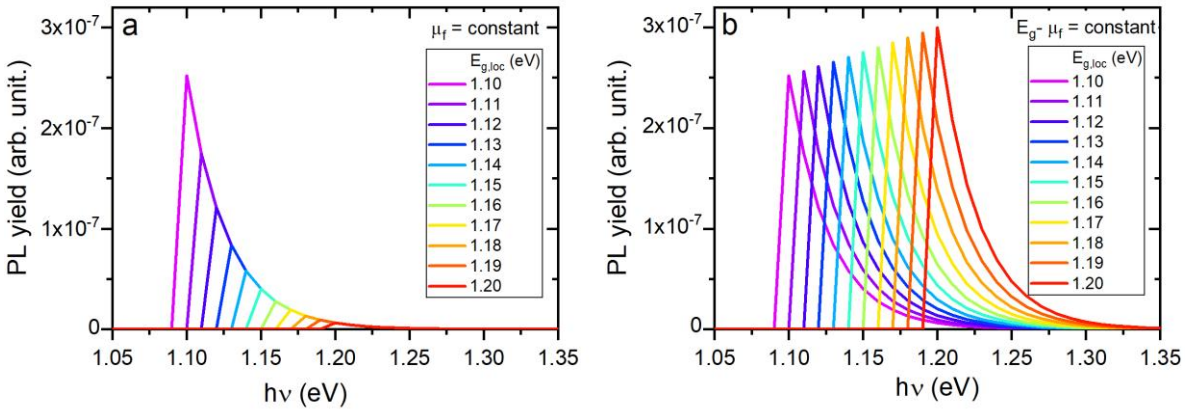

FIG. 2. Simulated PL spectra calculated with the LSW equation for band gap variations. a: small scale fluctuations with constant qfls. b: large scale fluctuations with the fermi level following the band gap.

B. Interference

Another feature affecting the shape of RT-PL spectra is the presence of interference. To see this in the PL spectra, the absorber layer needs to fulfill a few requirements. These are: 1) smooth surface i.e. a Ra of few 10s of nm, 2) the back interface needs to have high specular reflectivity and 3) the emitted light should not be re-absorbed. This can be the case if there are band gap gradients. For instance, the notch profile in 3-stage co-evaporated CIGS layers may cause interference in the spectra when the emission comes from the lowest band gap position i.e. the notch. In kesterite, the emission comes from below the band gap due to tail states and when the layer is sufficiently smooth interference may also be present. Both effects has been observed[11].

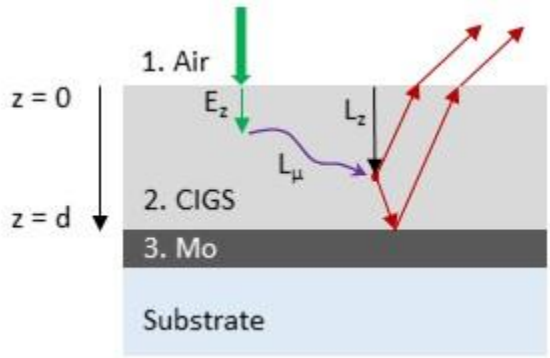

FIG. 3. Schematic overview of the parameters to calculate the IF function. E(z) is the excitation profile, L(z) the distribution of the luminescence centers. L_μ is the minority diffusion length. The numbers 1 ,2 ,3 correspond to the indices in eq. 4.

Interference associated with luminescence coming from within a layer is described by Holm et. al. [19]. Figure 3 gives a schematic overview of the relevant variables to calculate this interference spectrum. These are: 1) the position the carriers are excited i.e. the excitation profile $E(z)$, 2) the position where the carriers are recombining radiatively i.e. the luminescence center $L(z)$, the thickness of the layer d, and of course the refractive indices of the layers involved. The spatial difference between excitation of the carriers at position $E(z_e)$ and radiative recombination of the carriers at position $L(z_l)$ is given by the diffusion length of

the minority carriers L_μ. The resulting equation is called an interference function (IF). In here we give the function in the case the emitted light is perpendicular to the surface, removing the s and p polarization from the equations. The probability to emit at a certain position z is then given by:

$$P(\lambda) = \frac{1}{8\pi}\frac{n_2}{n_1}|t_{21}|^2 \frac{|1+r_{23}\exp(i\delta)|^2}{|1-r_{21}r_{23}\exp(i\varphi)|^2} \quad (4)$$

with $(r,t)_{ij}$ the complex reflection and transmission coefficients following from the Fresnel equations, $\delta = \frac{2\pi N_2}{\lambda}(2d-2z)$ and $\varphi = \frac{2\pi N_2}{\lambda}2d$. The indices ij, and d and z are as defined in Figure 3. N_2 is the complex refractive index of the CIGS layer, and n_2 and n_1 the real part of the refractive indices for CIGS and air respectively. To get the IF, the probability function needs to be integrated over the thickness of the absorber layer d, the excitation profile $E(z)$ and the luminescence centers $L(z)$. The integral is given by:

$$IF(\lambda) = \int_0^d L(z)E(z)P(\lambda)dz \quad (5)$$

The excitation profile depends on the absorption of the laser light and decays exponentially: $E(z) \propto \exp(-\alpha_{\lambda_{laser}} z)$. In the case of a Lambert-Beer emission profile $L(z) = 1$ and the emission depends only on the excitation profile. The IF follows closely the 1-R spectra in this case. When $L(z)$ is not 1 but localized, the IF minima and maxima are shifted compared to 1-R. Figure 4a gives the IFs of a 500 nm thin CIGS film for 4 cases: emission at the front $L(z) = \delta(z)$, emission 325 nm below the surface $L(z) = \delta(z-325)$, emission from the back $L(z) = \delta(z-500)$ and $L(z) = 1$. 1-R is also calculated and given for comparison. For $L(z) = 1$, $L(z) = \delta(z)$, and $L(z) = \delta(z-500)$ the position of the minima and maxima follow closely the 1-R spectra. When the emission comes from mid absorber layer, the minima and maxima are shifted compare to 1-R, as shown for $L(z) = \delta(z-325)$. The amplitude depends on the luminescent film thickness, which may vary between the absorber layer thickness and only an interface, and complex refractive index k. When the multiplication of the two is much smaller than 1, the amplitude increases accordingly due to contribution of wide angle interference[19]. This is the especially the case for $L(z) = \delta(z)$ showing an amplitude above unity.
In Figure 4b the corresponding normalized PL are given by multiplying the IFs with a Gaussian peak. While the peak minima and maxima are at the same position for front, back and $L(z) = 1$, the final PL spectra reveal larger differences. In these 3 situations, the PL peak maximum is shifted towards higher wavelengths and at lower wavelengths a second peak is observed. When the emission comes from about 325 nm below the surface, the peak maximum is shifted to lower wavelength and the second lower peak is at higher wavelengths. Thus, seemingly small shifts of the minima and maxima positions result in significant changes of the PL spectra. While interference is a known phenomenon in thin films, it is clearly enhanced in our ultrathin films. This can be explained by the presence of only 1 interference maximum/minimum overlapping with the undisturbed PL peak and the large contribution of wide-angle interference increasing the amplitude. When the fringe is then exactly positioned at the slope of the PL peak, drastic changes in the shape as observed in figure 4b are possible.

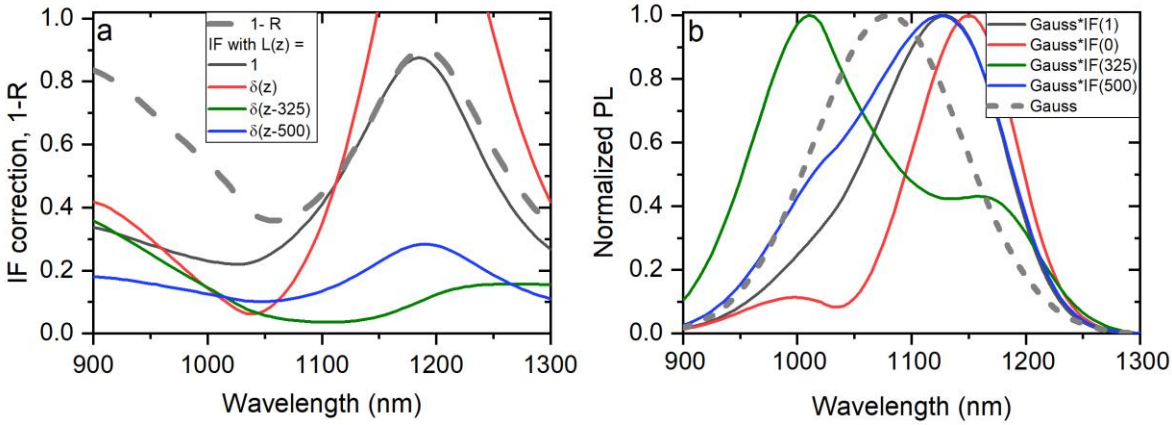

FIG. 4. a: calculated IFs with various L(z) and 1-R for a 500 nm thin CIGS layer on Mo. b: the resulting normalized PL spectra for the calculated IFs. Also, the undisturbed Gaussian peak is given.

III. EXPERIMENTAL

Ultrathin (~ 500 nm) samples were prepared by co-evaporation. For this we used a single stage process and a 3-stage process. The single stage process is described elsewhere and leads to grains of about 100 nm and a surface roughness Ra of 35 nm[20,21]. The 3-stage process is slightly adapted to get ultrathin layers and the layers have a roughness of about 100 nm. The composition and thickness of the samples were measured with XRF from which the band gap was determined. The CGI and GGI ratios were ~0.8 and ~0.3 for all the samples. The samples were covered with ~ 20 nm CdS deposited with chemical bath deposition. We applied the CdS layer as it is known to passivate the CIGS surface by implementing a favorable conductions band offset resulting in relative low interface recombination[22,23].

The intensity dependent PL spectra and decays were recorded at RT with a fluorescence spectrometer from Hamamatsu. The excitation wavelength was 532 nm with a 15 kHz, 1.2 ns pulsed laser. The spot size was about 30 mm^2 and the intensity was varied from 0.3 to 46 mW. One single stage sample was measured with hyper-spectral imaging to assess the (in)homogeneity of the layer. The global hyperspectral imager (IMA; Photon etc., Canada) consisted of an optical microscope coupled to a continuous wave laser, a broadband illumination source, and a hyperspectral filter based on volume Bragg gratings (VBG)[24]. The samples were homogeneously excited with a 532 nm laser, and the optical and PL images were acquired with an InGaAs camera. Spectrally and spatially resolved luminescence and reflectance images with a 3 nm spectral resolution and a 1 µm (diffraction-limited) spatial resolution were obtained.

The calculations of the reflection and band gap fluctuations were performed in origin software. The IFs were calculated in Python. The CdS layer of 20 nm was omitted in the calculations for two reasons. 1) The refractive indices are rather similar between CIGS and CdS in the NIR i.e. between 3.1-2.8 and 2.9-2.8 from 1000 to 1300 nm for CIGS and CdS respectively, and 2) the interface between the CIGS and CdS is not sharp as there is interdiffusion of Cu and Cd extending over a few nm's[25,26] and thus a gradient of refractive indices are expected here as well. Because the reflection at the CdS/CIGS interface in the NIR region is negligible, the CdS layer might add to the total thickness of the stack though. The undisturbed single stage spectra were approximated with a Gaussian peak and the interference function was calculated using a delta function for the localized luminescence center. The corrected spectra were modelled with the band gap fluctuations model by varying σ_g and β until the model fitted the measured spectra.

IV. RESULTS

A. Single stage spectra

The PL spectra of single-stage samples appear to consist of 2 peaks. In earlier contributions, In/Ga separation and secondary phases were eliminated by GDOES and XRD[13]. Another reason for an extra peak in the PL spectra is the presence of interference as described above. One single stage sample was measured with hyperspectral imaging to obtain a map with lateral microscopic resolution of the PL and reflection spectra. In Figure 5 the obtained maps with the individual reflection and PL spectra are presented. Figure 5a gives the maximum intensity of the reflection at 1050 nm. The reflection spectra are shown in Figure 5b for the average value (full area), and for a high and low count spot. We find that the reflection is very homogeneous on this µm scale. In Figure 5c, a map of the PL intensity at 1050 nm is given and, in Figure 5d, the individual spectra. Like the reflection spectra, there are seemingly large differences in intensity from the color map. However, when looking at the individual spectra, we find that the intensity varies about a factor of 1.5. This is lower than observed in other groups for the thick layers[17,18]. When looking at those 2 maps, there is no correlation visible between the light and dark areas. Figure 5e shows the PL peak maximum after 5 points smoothing of each individual spectrum. Also, here the variations seem random and no features can be observed. When making a histogram of the number of pixels belonging to a certain wavelength range, we observe a Gaussian distribution. This is presented in Figure 5f. Since the variations in the PL peak maximum follow a Gaussian distribution, they are likely real microscale variations of the band gap. The FWHM is 23 meV, the variations of the peak maxima extracted from the wavelength range in Figure 5e is 42 meV. If the lateral fluctuations are smaller than 1 µm this can be interpreted as a lower limit of the amount of fluctuations, since the various band gaps cannot be resolved beyond 1 µm. From the simulations in section A, we have seen that when the intensity of the PL yield marginally changes, the scale of the fluctuations is large compared to the diffusion length. We have variations of about 1.5, indicating slightly intermediate to large scale band gap fluctuations with an upper limit of 1 µm for the lateral fluctuations and a diffusion length smaller than 1 µm.

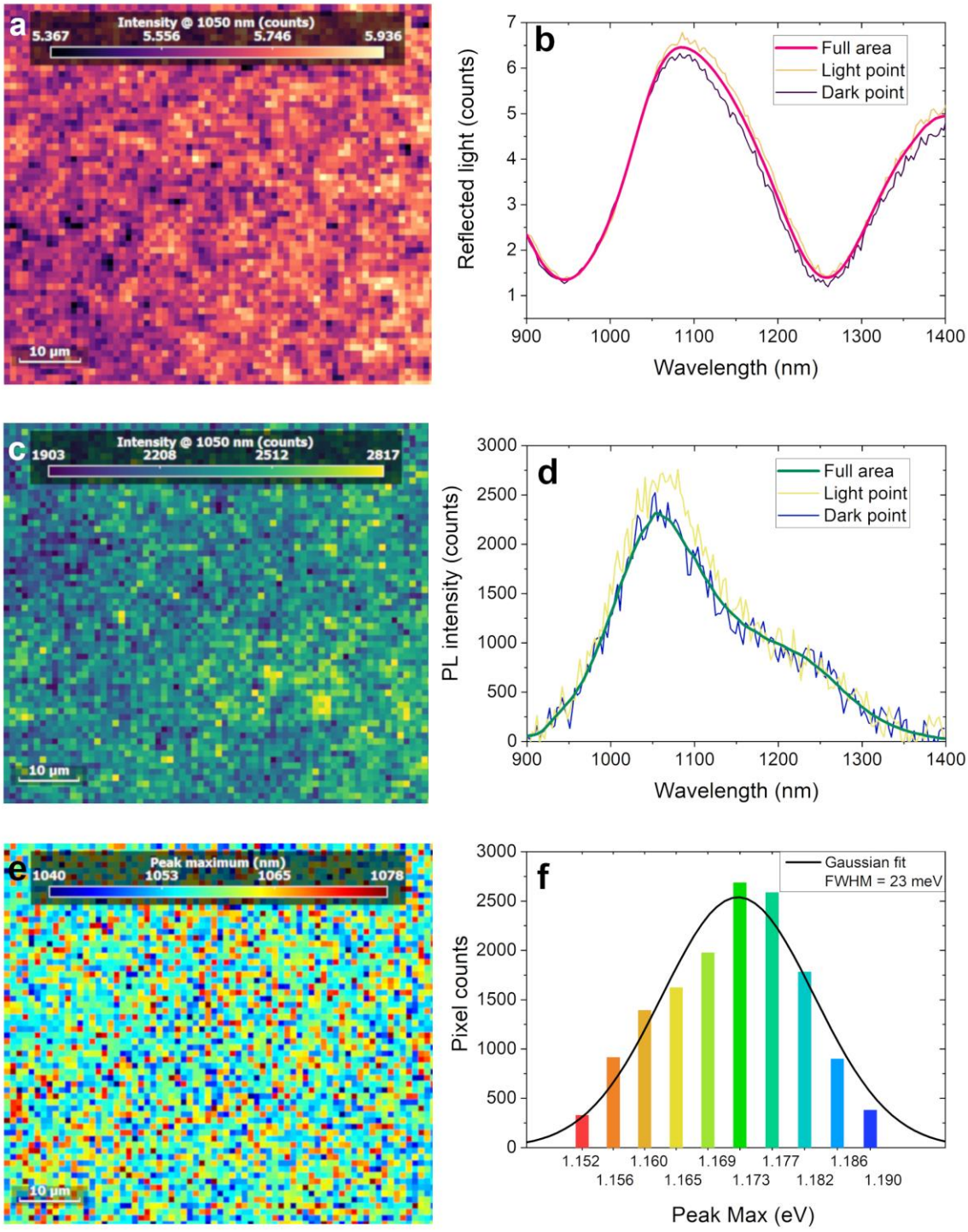

FIG. 5. Hyperspectral data from the single stage sample. a: intensity map of the reflection at 1050 nm, b: individual spectra. c: intensity map of the PL yield at 1050 nm, d: individual spectra. e: map of thr PL max (5 points smoothed), f: histogram of the pixels per energy of the PL peak, fitted with a Gaussian distribution.

B. Blueshift

The second observation we will discuss here, is the blueshift of the PL spectra upon increasing carrier injection at RT. The blueshift is observed for both 3-stage as single stage CIGS samples. We will first present the data of an ultrathin 3-stage sample as the 3-stage sample has only one peak. The measured and modelled spectra and decays are presented in Figure 6a and b. Next

to the blueshift, we observed that the decays decrease upon increasing power intensity. A blueshift at room temperature is generally not observed as the band gap should not change upon carrier injection. However, the band gap fluctuations model has a parameter β that shifts the peak away from the mean band gap if β is smaller than 1. This means that the scale of the band gap fluctuations is smaller than or similar to the diffusion length. To fit the data presented in Figure 6a, the band gap was set at 1.18 eV based on an average CGI of ~ 0.3 and the β was adapted accordingly. The σ_g was kept constant, as the local band gaps should also not be impacted by increased carrier injection. The measured peaks, the modelled spectra and the parameters to fit curves are shown in Figure 6a as well. The σ_g extracted was 45 meV and the β increased from 0.64 to 1 for increasing carrier injection. Thus, an increase in β can explain the blueshift.

This change in β can be explained when looking at eq. 2. We see that β depends on the diffusion length L_μ as well as the scale of the band gap fluctuations L_g. Since the band gap depends on the composition, it is unlikely that L_g changes upon increasing carrier injection and hence, we assume it to be constant. The diffusion length however, depends on the lifetime via the relationship $L_\mu \propto \sqrt{D\tau}$, which decreases upon carrier injection as shown in figure 6b. Since $\beta \propto 1/L_\mu^2 \propto 1/\tau$, it follows that β increases when τ decreases. This is exactly what we observed: a decrease in τ and an increase in β resulting in the blueshift of the PL spectra. It has to be mentioned that this only holds when β is between 0 and 1, which means that the band gap fluctuations must be of the same order as or slightly larger than the diffusion lengths i.e. $L_\mu \sim L_g$. An upper limit of the scale of the fluctuations can be deduced from the extracted lifetime of about 2-3 ns. Using an electron mobility of 50 cm^2Vs^{-1} [17,18,22], a diffusion length of about 0.6 µm is calculated.

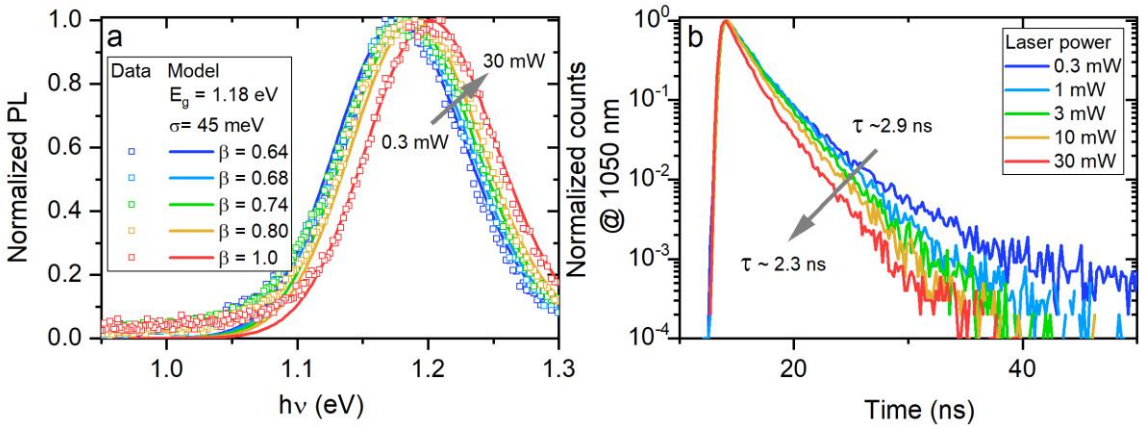

FIG. 6. a: intensity dependent PL spectra and b: decays for the 3-stage sample. The spectra are modelled with the band gap fluctuations model and parameters are given in the graph. On the right the extracted decay time for the lowest and highest power are given.

The blueshift has also been observed in the single stage spectra, however due to the interference also the peak shape changes. To understand the effect of seemingly shifting interference fringes in our single stage PL spectra, we will model the anomalous behavior that was observed for the single-stage samples upon intensity dependent measurements. The PL spectra for one of the most extreme case we observed is shown in Figure 7a. To model these spectra, we used 1-R as an interference function and applied a change in β to simulate the increase in laser power. 1-R and σ_g were kept constant. The modelled spectra are presented in Figure 7b. The parameters used to model this, are given as well. The change in β upon carrier injection combined with interference fringes can thus explain the anomalous peak shifts seen in the single stage spectra. However, to model this, the band gap was about 100 meV higher than

would be expected for a single stage layer with a CGI of 0.3. This will be addressed later. First, we will explore the options to correct the single stage spectra for the interference fringes.

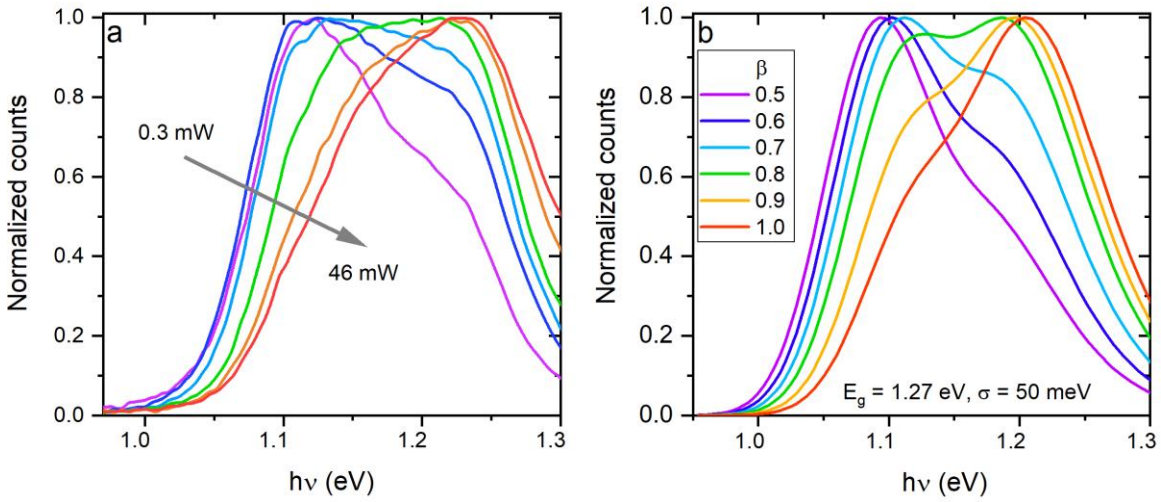

FIG. 7. a: intensity dependent measurement of a single stage sample. b: modelled PL with changing β and interference.

C. Correction for interference

To extract the band gap fluctuations of the single stage grown absorber layer, the spectra needs to be corrected for the interference fringes. In here we compare two correction methods based on measured reflection spectra and a calculated IF (eq.4 and 5). To model the measured spectra we used a Gaussian function to model the PL peak without interference and multiplied it with a yet to determine IF from the reflection spectra. At first, we used 1-R as an IF, thus the fringes follow the IF with $L(z) = 1$, which is expected as there is no notch profile. The measured and calculated PL spectra are presented in Figure 8a. We clearly see that interference fringes are not correctly positioned. It seems therefore that the fringes need to be shifted over a certain wavelength range λ. This is presented in the Figure 8b. When shifting 1-R over a range λ and multiply R with a constant >1, we get a good match with the spectra. However, a shift of 1-R over a wavelength range λ implies a localized emission center i.e. $L(z) = \delta(z - z_{loc})$. To get an estimate from where the emission comes from, we also calculated the IF that fits the measured spectra. The thickness of the layer was 490 nm, the emitted light perpendicular to the surface and the band gap 1.16 eV. The simulated PL spectra is shown in Figure 8c. We find a good match when $L(z) = \delta(z - 117)$. This implies that the emission comes from about 117 nm below the surface. While localized emission is unexpected as there is no notch profile, it can be explained by the low decay time. The decay of a single stage sample is typically below 1 ns[20], corresponding to a diffusion length of a few 100 nm. As most of the carriers are excited at the front, and then diffuse about 100 nm and more, it can explain why the emission seems to appear from this position.

Correction of the interference fringes can then be easily done by dividing the measured data by the experimentally determined interference function. Figure 9a shows the corrected PL spectrum when the IF was determined from the reflection spectra and Figure 9b the resulting PL spectrum when corrected with the calculated IF. The corrected PL spectra can then be modelled with the band gap fluctuations model which was done for both correction methods. We find a σ_g of 74 and 69 meV and a β of 0.58 and 0.52 for the reflection corrected and IF calculated PL spectra respectively. There are small variations in the values, but close enough to conclude that the band gap fluctuation is about 72 ± 3 meV for the single stage sample. This

is larger than the 45 meV for the 3-stage sample, despite not having a Ga gradient. The β is between 0 and 1, which is to be expected for intermediate scale band gap fluctuations.

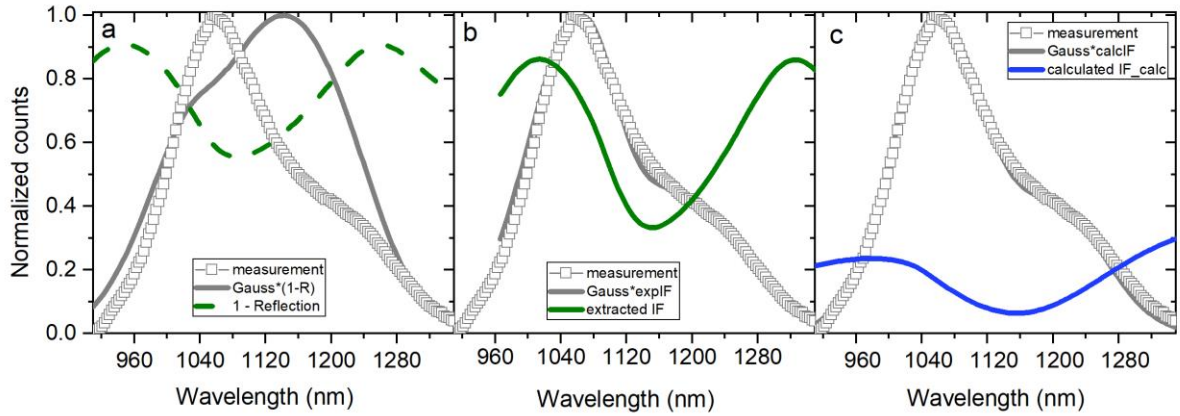

FIG. 8. Single stage PL spectrum from the hyper spectral response (squared data). The PL spectra are simulated with a Gaussian distribution*IF to fit the measured data. a: IF = 1-R, b: IF = 1-R shifted over a wavelength range λ and c: IF calculated and L(z) adapted.

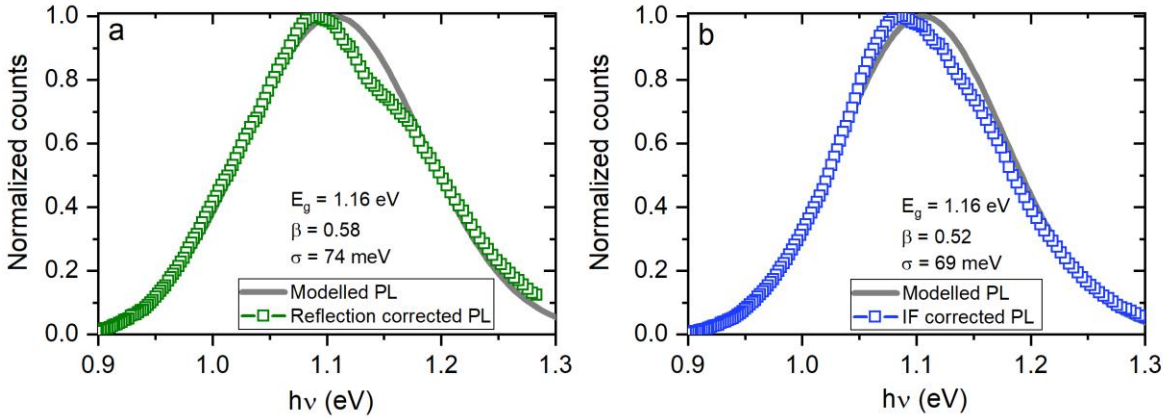

FIG. 9: Single stage spectra corrected for interference fringes (squared data). a: correction from reflection measurement, b: correction from calculated IF. The resulting spectra are modelled with band gap fluctuations to extract the σ_g and β (grey lines).

V. DISCUSSION

The photoluminescence spectra of ultrathin CIGS samples exhibit intermediate scale band gap fluctuations. This means that the lateral scale of the band gap fluctuations is only slightly larger than the diffusion length. The diffusion length in our samples is estimated to be a few 100 nm. It has to mentioned that more models are available to describe the RT PL. Katahara et. al, has developed a comprehensive model based on varying sub band gap absorption profiles[16]. From these models the PL spectra can be simulated and the origin of broadening deduced, but it cannot explain the blueshift observed in our data. It may explain though the PL further below the band gap, like observed in Figure 6a. Here we see that the PL data and model starts to deviate, which may imply that this emission is indeed due to tail states below the band gaps. One of the models, described the presence of potential fluctuations. As CIGS is known to be limited by potential fluctuations[27], it is possible that the low energy tail may be due to this. However, most of the peak and the blueshift can be described by band gap fluctuations as evident from the modelling in Figure 6a. It is worth mentioning that the finding that τ decreases

upon increasing carrier injection, can also be explained by the presence of potential fluctuations. Potential fluctuations arise at locations with charged defects and are mainly present at grain boundaries and other dislocations. They may also result in barriers for minority or majority carriers reducing recombination at these charged defects. As these barriers can reduce upon increasing carrier injection the recombination at these charged defects will increase and thus the decay time will decrease. We find lower decay times for the single stage sample, which could be attributed to a higher amount of potential fluctuations.

The origin of the band gap fluctuations is often attributed to differences in compositions. These compositional variations can occur on sub nanometer to sub µm scale[28]. While the mean value of the scale of the band gap fluctuation should be slightly larger than the diffusion length, nm scale variations are not necessarily excluded to contribute to the band gap fluctuations. In a 3-stage sample there is an (unintentionally) Ga gradient, and the bandgap fluctuations can be attributed to this gradient. However, in here we have shown that the band gap fluctuations are significantly larger for a sample without a Ga gradient and thus the fluctuations must have another source. The main difference between 3-stage and single stage growth, besides the Ga gradient, is the presence of a copper rich stage. This copper rich stage increases the grainsize and annihilates the planar defects inside the grain[29,30]. We hypothesize that these structural defects may increase the band gap fluctuations in the copper poor grown layer compared to the copper rich grown layer. Since grain boundaries and planar defects are more present in the single stage sample than in the 3-stage sample due to the smaller grain size, we hypothesize that the larger band gap fluctuations origin from these structural defects. Additionally, it follows from the higher number of structural defects that the potential fluctuations in single stage CIGS are more significant and therefore may also broaden the PL spectra.

The single stage sample did not only exhibit more band gap fluctuations than the 3-stage sample but was also drastically affected by interference. Correction for the interference fringe was done by calculating the IF. However, to match the interference fringes with those measured in the PL spectra the IF required to be localized. It was determined that the emission must come from about 117 nm deep in the absorber layer. While the corrected spectra still showed some small anomalies, and thus the modelling require some improvements, the conclusion that the emission comes from deeper in the absorber layer remains. This implies a so-called dead zone at the front[19]. This dead zone can mean that in that area the recombination is not radiative or that the carriers simply do not recombine in that area. The latter could be the case in the space charge region (SCR) of a solar cell, where the recombination is significantly lower than in the neutral region. Since we do have a CdS layer, we might have a SCR. It is found that CIGS/CdS has a buried homojunction about 50 to 100 nm below the surface[31]. However, this buried junction is not exclusively assigned to the presence of a CdS layer, but also to a copper depleted surface[32]. Nevertheless, the CdS layer will affect the IF as there will be a redistribution of the carriers compared to the absence of the buried junction. Earlier research has already shown changes in PL spectra after CdS deposition[33]. Therefore, careful determination of IFs of various layers with and without CdS layer and various distribution of L(z) is under investigation and may shed light on the origin of the dead zone in single stage absorber layers.

VI. SUMMARY

Ultrathin co-evaporated layers were analyzed by room temperature photoluminescence measurements. We found that the ultrathin layers exhibit band gap fluctuations on the scale of the diffusion length, causing a blue shift upon increasing carrier injection. Additionally, single stage grown layers have interference fringes which should be corrected for. These fringes do not follow the 1-R spectra, which would be expected from a sample without any Ga gradient.

However, by calculating the IF it appears that the emission comes from about 100 nm and deeper in the absorber layer. This is probably due to the low decay time (indistinguishable from the IRF), indicating a diffusion length of about a few 100 nm. The band gap fluctuations extracted for the single stage spectra was larger than for the 3-stage spectra. Potential reasons for the difference between the single stage and 3-stage samples are given as well.

ACKNOWLEDGEMENTS

This work received funding from the European Union's H2020 research and innovation program under grant agreement No. 715027. We thank Photon etc. and Prof. Delphine Bouilly's research group from IRIC for the hyperspectral measurements and MSc Erik Spaans for the python program.

DATA AVAILABILITY

The data that support the findings of this study are available from the corresponding author upon reasonable request.

[1] S. Siebentritt, in *Wide-Gap Chalcopyrites*, edited by S. Siebentritt and U. Rau (Springer, Berlin, Heidelberg, 2006), pp. 113–156.
[2] T. Unold and L. Gütay, in *Advanced Characterization Techniques for Thin Film Solar Cells* (John Wiley & Sons, Ltd, 2016), pp. 275–297.
[3] F. Babbe, L. Choubrac, and S. Siebentritt, Solar RRL **2**, 1800248 (2018).
[4] G. Rey, C. Spindler, F. Babbe, W. Rachad, S. Siebentritt, M. Nuys, R. Carius, S. Li, and C. Platzer-Björkman, Phys. Rev. Applied **9**, 064008 (2018).
[5] U. Rau and J.H. Werner, Appl. Phys. Lett. **84**, 3735 (2004).
[6] J. Mattheis, U. Rau, and J.H. Werner, Journal of Applied Physics **101**, 113519 (2007).
[7] S. Siebentritt, G. Rey, A. Finger, D. Regesch, J. Sendler, T.P. Weiss, and T. Bertram, Solar Energy Materials and Solar Cells **158**, 126 (2016).
[8] D. Colombara, F. Werner, T. Schwarz, I. Cañero Infante, Y. Fleming, N. Valle, C. Spindler, E. Vacchieri, G. Rey, M. Guennou, M. Bouttemy, A.G. Manjón, I. Peral Alonso, M. Melchiorre, B. El Adib, B. Gault, D. Raabe, P.J. Dale, and S. Siebentritt, Nature Communications **9**, 826 (2018).
[9] Ö. Demircioğlu, J.F.L. Salas, G. Rey, T. Weiss, M. Mousel, A. Redinger, S. Siebentritt, J. Parisi, and L. Gütay, Opt. Express, OE **25**, 5327 (2017).
[10] A. Lomuscio, T. Rödel, T. Schwarz, B. Gault, M. Melchiorre, D. Raabe, and S. Siebentritt, Phys. Rev. Applied **11**, 054052 (2019).
[11] J.K. Larsen, S.-Y. Li, J.J.S. Scragg, Y. Ren, C. Hägglund, M.D. Heinemann, S. Kretzschmar, T. Unold, and C. Platzer-Björkman, Journal of Applied Physics **118**, 035307 (2015).
[12] J. de Wild, T. Kohl, D.G. Buldu, G. Birant, D.M. Parragh, G. Brammertz, M. Meuris, J. Poortmans, and B. Vermang, in *2019 IEEE 46th Photovoltaic Specialists Conference (PVSC)* (2019), pp. 0928–0930.
[13] J. de Wild, D.G. Buldu, T. Schnabel, M. Simor, T. Kohl, G. Birant, G. Brammertz, M. Meuris, J. Poortmans, and B. Vermang, ACS Appl. Energy Mater. **2**, 6102 (2019).
[14] G. Lasher and F. Stern, Phys. Rev. **133**, A553 (1964).
[15] P. Wurfel, J. Phys. C: Solid State Phys. **15**, 3967 (1982).
[16] J.K. Katahara and H.W. Hillhouse, Journal of Applied Physics **116**, 173504 (2014).

[17] F. Heidemann, R. Brüggemann, and G.H. Bauer, J. Phys. D: Appl. Phys. **43**, 145103 (2010).
[18] A. Delamarre, M. Paire, J.-F. Guillemoles, and L. Lombez, Progress in Photovoltaics: Research and Applications **23**, 1305 (2015).
[19] R.T. Holm, S.W. McKnight, E.D. Palik, and W. Lukosz, Appl. Opt., AO **21**, 2512 (1982).
[20] J. de Wild, M. Simor, D.G. Buldu, T. Kohl, G. Brammertz, M. Meuris, J. Poortmans, and B. Vermang, Thin Solid Films **671**, 44 (2019).
[21] T. Kohl, N.A. Rivas, J. de Wild, D.G. Buldu, G. Birant, G. Brammertz, M. Meuris, F.U. Renner, J. Poortmans, and B. Vermang, ACS Appl. Energy Mater. **3**, 5120 (2020).
[22] T.P. Weiss, B. Bissig, T. Feurer, R. Carron, S. Buecheler, and A.N. Tiwari, Scientific Reports **9**, 5385 (2019).
[23] M. Gloeckler and J.R. Sites, Thin Solid Films **480**–**481**, 241 (2005).
[24] C.O.R. Quiroz, L.-I. Dion-Bertrand, C.J. Brabec, J. Müller, and K. Orgassa, Engineering (2020).
[25] P.M.P. Salomé, R. Ribeiro-Andrade, J.P. Teixeira, J. Keller, T. Törndahl, N. Nicoara, M. Edoff, J.C. González, J.P. Leitão, and S. Sadewasser, IEEE Journal of Photovoltaics **7**, 858 (2017).
[26] T. Nakada and A. Kunioka, Appl. Phys. Lett. **74**, 2444 (1999).
[27] S. Siebentritt, Solar Energy Materials and Solar Cells **95**, 1471 (2011).
[28] D. Abou-Ras, N. Schäfer, C.J. Hages, S. Levcenko, J. Márquez, and T. Unold, Solar RRL **2**, 1700199 (2018).
[29] P.M.P. Salomé, V. Fjällström, P. Szaniawski, J.P. Leitão, A. Hultqvist, P.A. Fernandes, J.P. Teixeira, B.P. Falcão, U. Zimmermann, A.F. da Cunha, and M. Edoff, Progress in Photovoltaics: Research and Applications **23**, 470 (2015).
[30] R. Mainz, E.S. Sanli, H. Stange, D. Azulay, S. Brunken, D. Greiner, S. Hajaj, M.D. Heinemann, C.A. Kaufmann, M. Klaus, Q.M. Ramasse, H. Rodriguez-Alvarez, A. Weber, I. Balberg, O. Millo, P.A. van Aken, and D. Abou-Ras, Energy Environ. Sci. **9**, 1818 (2016).
[31] C.-S. Jiang, F.S. Hasoon, H.R. Moutinho, H.A. Al-Thani, M.J. Romero, and M.M. Al-Jassim, Appl. Phys. Lett. **82**, 127 (2002).
[32] Y. Okano, T. Nakada, and A. Kunioka, Solar Energy Materials and Solar Cells **50**, 105 (1998).
[33] D.G. Buldu, J. de Wild, T. Kohl, G. Birant, G. Brammertz, M. Meuris, J. Poortmans, and B. Vermang, in *2019 IEEE 46th Photovoltaic Specialists Conference (PVSC)* (2019), pp. 0920–0922.